ADVANCED MATERIALS
www.advmat.de

Critical-Layered MoS_2 for the Enhancement of Supercontinuum Generation in Photonic Crystal Fibre

Jin Xie, Xu Cheng, Guodong Xue, Xiao Li, Ding Zhong, Wentao Yu, Yonggang Zuo, Chang Liu, Kaifeng Lin, Can Liu, Meng Pang, Xin Jiang, Zhipei Sun, Zhe Kang, Hao Hong,* Kaihui Liu,* and Zhongfan Liu**

Supercontinuum generation (SCG) from silica-based photonic crystal fibers (PCFs) is of highly technological significance from microscopy to metrology, but has been hindered by silica's relatively low intrinsic optical nonlinearity. The prevailing approaches of filling PCF with nonlinear gases or liquids can endow fibre with enhanced optical nonlinearity and boosted SCG efficiency, yet these hybrids are easily plagued by fusion complexity, environmental incompatibility or transmission mode instability. Here this work presents a strategy of embedding solid-state 2D MoS_2 atomic layers into the air-holes of PCF to efficiently enhance SCG. This work demonstrates a 4.8 times enhancement of the nonlinear coefficient and a 70% reduction of the threshold power for SCG with one octave spanning in the MoS_2-PCF hybrid. Furthermore, this work finds that the SCG enhancement is highly layer-dependent, which only manifests for a real 2D regime within the thickness of five atomic layers. Theoretical calculations reveal that the critical thickness arises from the trade-off among the layer-dependent enhancement of the nonlinear coefficient, leakage of fundamental mode and redshift of zero-dispersion wavelength. This work provides significant advances toward efficient SCG, and highlights the importance of matching an appropriate atomic layer number in the design of functional 2D material optical fibers.

1. Introduction

Supercontinuum generation (SCG) light source, with the capability of producing ultra-broadband coherent radiation, have been widely used in various applications including ultrafast spectroscopy, super-resolution optical microscopy, optical coherence tomography, frequency comb technology and optical telecommunications.[1–7] Generally, SCG originates essentially from the fundamental processes of self-phase modulation (SPM) and soliton dynamics, with the control of dispersion, loss and nonlinear coefficient of the medium ($\gamma = \frac{2\pi}{\lambda}\frac{n_2}{A_{\text{eff}}}$, where λ is the wavelength, n_2 is the nonlinear refractive index, and A_{eff} is the effective mode area determined by the waveguide structure and material properties). The conventional commercial SCG light sources, with spectral coverage from the visible to near-infrared spectrum are predominantly relies on silica-based photonic crystal fibre (PCF)

J. Xie, G. Xue, X. Li, C. Liu, K. Lin, H. Hong, K. Liu
State Key Laboratory for Mesoscopic Physics, Frontiers Science Center for Nano-optoelectronics, School of Physics
Peking University
Beijing 100871, China
E-mail: haohong@pku.edu.cn; khliu@pku.edu.cn

J. Xie, G. Xue, X. Li, K. Lin
Academy for Advanced Interdisciplinary Studies
Peking University
Beijing 100871, China

J. Xie, Z. Liu
Beijing Graphene Institute (BGI)
Beijing 100095, China
E-mail: zfliu@pku.edu.cn

X. Cheng
Group for Fibre Optics
École Polytechnique Fédérale de Lausanne (EPFL)
Lausanne 1015, Switzerland

The ORCID identification number(s) for the author(s) of this article can be found under https://doi.org/10.1002/adma.202403696

DOI: 10.1002/adma.202403696

X. Cheng
Haute Ecole ARC Ingénierie
University of Applied Sciences of Western Switzerland
Saint-Imier 2610, Switzerland

D. Zhong, C. Liu
Department of Physics
Renmin University of China
Beijing 100872, China

W. Yu
Institute of Interdisciplinary Physical Sciences, School of Physics
Nanjing University of Science and Technology
Nanjing 210094, China

Y. Zuo
Faculty of Metallurgical and Energy Engineering
Kunming University of Science and Technology
Kunming 650093, China

M. Pang, X. Jiang
Innovation and Integration Center of New Laser Technology, Shanghai Institute of Optics and Fine Mechanics
Chinese Academy of Sciences
Shanghai 201800, China

with tunable dispersion profile, low-loss transmission ability and devisable A_{eff}, profiting from the well-established silica-based fibre fabrication technique.[8–13] However, the limited nonlinear refractive index of fused silica ($n_2 \approx 10^{-20}$ m^2 W^{-1}) poses fundamental limitations of the SCG light source on pump threshold and frequency-conversion efficiency, requiring high pumping power and long distance for strong light-matter interaction.

Apart from exchanging the base material of PCF (such as soft glass, with higher n_2 but more complex fabrication process) to enhance the efficiency of SCG,[13–18] previous efforts also employed nonlinear fluids (such as liquids and gases).[19–24] in a well-designed silica-based optical fibre. Gas-filled fibers offer the advantages of low absorption and tunable dispersion, enabling the SCG in an ultrabroad band ranging from vacuum ultraviolet to long-wave infrared band. Liquid-filled fibers provide higher nonlinearity, allowing the novel soliton dynamics with lower incident power. However, both hybrid fibers also face some challenges, such as the requirement of a sealed cell, the risk of material leakage, all-fibre integration and the instability against environmental vibration. In addition to these two strategies, an appealing alternative is to decorate silica-based PCFs with conventional solid optical crystals with highly nonlinear susceptibility, which would be for enhancing the nonlinear coefficient of the PCF and preserve its stability and portability for table-top laser sources. Nevertheless, depositing conventional solid-state crystals onto the curved surface of fibre holes will inevitably lead to scattering loss and mode leakage, due to the rough interface and the refractive index mismatch between adhered crystal and optical fibre.

M. Pang, X. Jiang
Russell Centre for Advanced Lightwave Science
Shanghai Institute of Optics and Fine Mechanics and Hangzhou Institute of Optics and Fine Mechanics
Hangzhou 311421, China

Z. Sun
QTF Center of Excellence, Department of Electronics and Nanoengineering
Aalto University
Espoo 02150, Finland

Z. Kang
Centre for Optical and Electromagnetic Research, College of Optical Science and Engineering, National Engineering Research Center for Optical Instruments, Ningbo Innovation Center
Zhejiang University
Hangzhou 310058, China
E-mail: zhe_kang@zju.edu.cn

H. Hong
Interdisciplinary Institute of Light-Element Quantum Materials and Research Centre for Light-Element Advanced Materials
Peking University
Beijing 100871, China

K. Liu
Songshan Lake Materials Lab, Institute of Physics
Chinese Academy of Sciences
Dongguan 523808, China

Z. Liu
Center for Nanochemistry, College of Chemistry and Molecular Engineering
Peking University
Beijing 100871, China

In principle, 2D layered materials (e.g., graphene, MoS_2, hBN, etc.),[25–30] with the merits of ultra-high optical nonlinear response (n_2 of MoS_2 film is about 4–5 orders of magnitude higher than that of silica at 1550 nm.),[31,32] atomic-level flatness (with low scattering loss).[33] extremely thin thickness (hardly damage the transmission mode),[34,35] and facile integration with silica-based waveguides,[36,37] are an ideal partner to combine with various waveguides for optical nonlinearity enhancement.[38] By transferring nonlinear 2D materials onto silica waveguides or fibers, optical nonlinear effects such as saturable absorption.[39] second-/third-harmonic generation (SHG/THG),[40,41] Kerr effect,[36] and SPM.[42] can be dramatically enhanced. Since the SPM plays a crucial role in the initial process of SCG, the combination of nonlinear 2D materials with PCF could be a promising strategy to improve the efficiency of SCG. Guided by these inspirations, here we directly grow solid-state thin-layer 2D MoS_2 onto the inner walls of air-holes of PCF (MoS_2-PCF) and systematically study its SCG performance. We find that the physical properties of PCF, including the γ, zero-dispersion wavelength (ZDW) and the fundamental mode distribution, can be gently engineered by the layer number of MoS_2. A real 2D regime within a critical thickness of around five-atomic-layer is required for strong SCG enhancement, bringing a 70% reduction in the threshold power to achieve one octave broadening.

2. Results and Discussion

In our work, MoS_2-PCF is designed with MoS_2 layers tightly attached on the inner walls of the air-holes of a silica-based nonlinear PCF (**Figure 1**a,b, and Figure S1, Supporting Information). According to the simulation result based on the full-vector finite element method.[43] the electric field intensity of the transmitted light at the innermost MoS_2 layer is ≈15% of that at the core centre, indicating a considerable light-MoS_2 interaction through the evanescent wave (Figure 1b,c and Experimental Section). To assess the SCG performance in PCF with the integration of MoS_2, we carefully evaluate three important parameters: dispersion, nonlinear coefficient and propagation loss in the following. Regarding the dispersion, we perform mode analysis of the proposed hybrid PCF and show that, except for a ≈8 nm redshift (from 797 to 805 nm) of the ZDW, the overall dispersion profile of monolayer MoS_2-PCF is nearly identical to that of the bare-PCF (Figure 1d). The large variation of the dispersion value ≈680 nm is attributed to the fluctuation of the real part of refractive index in MoS_2 induced by the exciton effects close to its bandgap (Figure S2, Supporting Information).[44–46]

As for γ in the MoS_2-PCF, it can be described as (Note S1, Supporting Information):

$$\gamma_{MoS_2-PCF} = \frac{2\pi}{\lambda} \frac{\sum_i \iint_{D_i} (n_2)_i (n_0^2)_i \left|F(x,y)\right|^4 dxdy}{\left(\sum_i \iint_{D_i} (n_0)_i \left|F(x,y)\right|^4 dxdy\right)^2} \quad (1)$$

where λ is the pump wavelength, $|F(x, y)|$ is the amplitude of electric field distribution of fundamental mode, D_i represents different integral areas, n_0 and n_2 are the linear and nonlinear refractive indices, respectively. With MoS_2 embedded, γ is remarkably

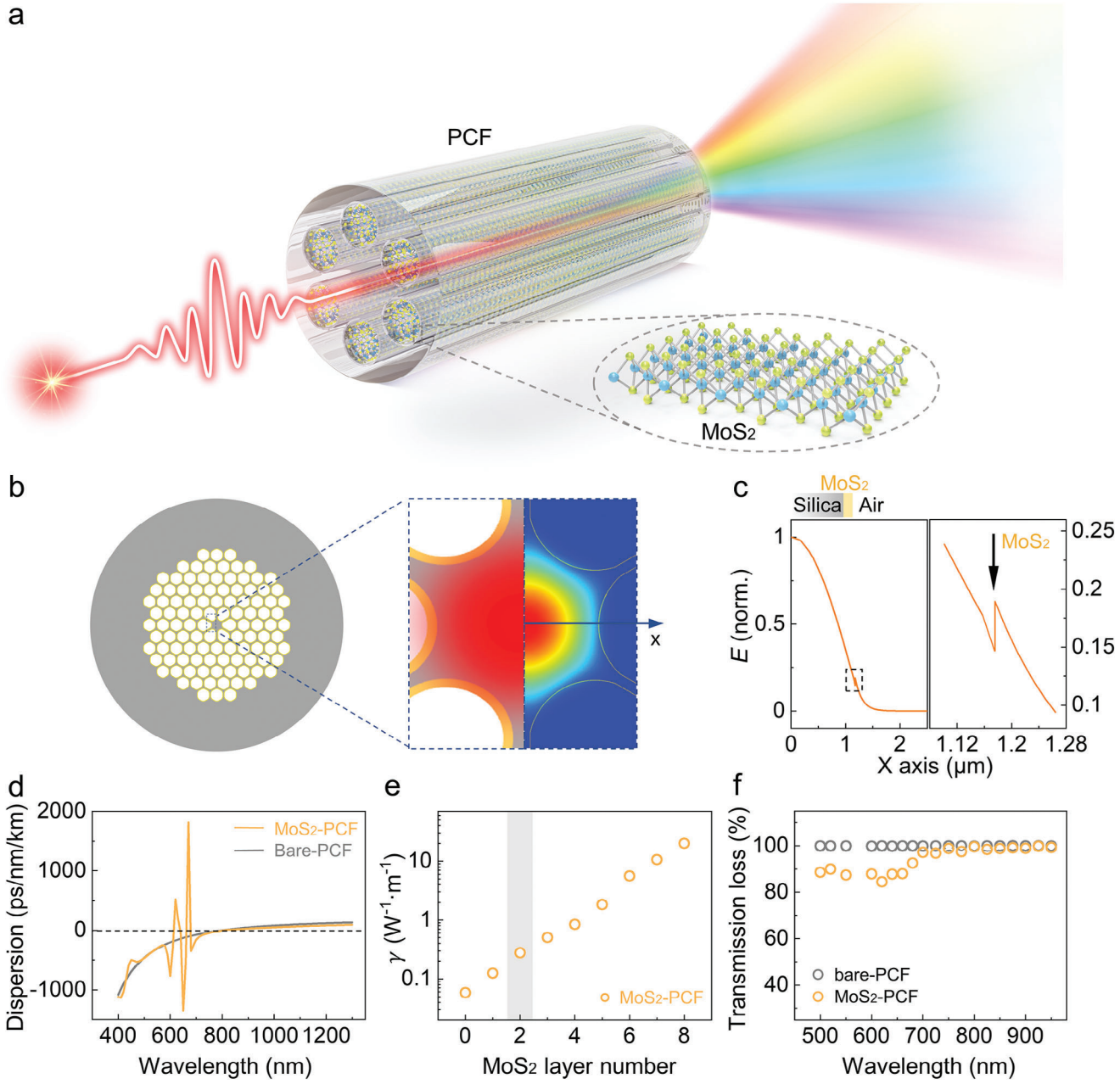

Figure 1. Optical properties of MoS_2-PCF. a) Schematic illustration of the SCG in PCF embedded with MoS_2 film. b) Cross-section illustration of the MoS_2-PCF structure. MoS_2 film is attached on the wall of air-holes in the PCF. The enlarged view is the spatial distribution of the fundamental mode around the core region at the 800 nm pump. c) Normalized electric field intensity distribution of MoS_2-PCF along the x-axis shown in Figure 1b. The electric field intensity at the innermost MoS_2 layer is ≈15% to that at the core centre, indicating a considerable light-MoS_2 interaction. d) Dispersion profile of the bare- and monolayer MoS_2-PCF. e) Layer-dependent nonlinear coefficient in MoS_2-PCF. Nonlinear coefficient of the hybrid PCF increases monotonously with the MoS_2 layer number. The grey shaded area indicates the layer number of thin-layer MoS_2-PCF used in the following experiments. f) The transmittance spectra of 3 cm bare-PCF and thin-layer MoS_2-PCF. The addition of MoS_2 hardly influence the transmittance of PCF.

boosted (highly correlated with the PCF structure, as calculated in Figure S3, Supporting Information) and increases gradually with the number of MoS_2 layers (Figure 1e). This layer-dependent behavior is ascribed to the enhanced light-MoS_2 interaction, as the increased thickness of MoS_2 layers brings more significant evanescent wave along the interaction path (Figure S4, Supporting Information). It is worth noting that via replacing the MoS_2 thin-layer by other 2D materials with larger third-order susceptibility, such as graphene or hBN,[47,48] could demonstrate a further enhancement of nonlinear coefficient (Figure S5, Supporting Information). However, the graphene one would suffer from a large transmission loss problem while the synthesis of hBN one is still challenging. From our experimental result, the additional loss induced by the quasi-bilayer MoS_2 in a 3 cm-long hybrid PCF is less

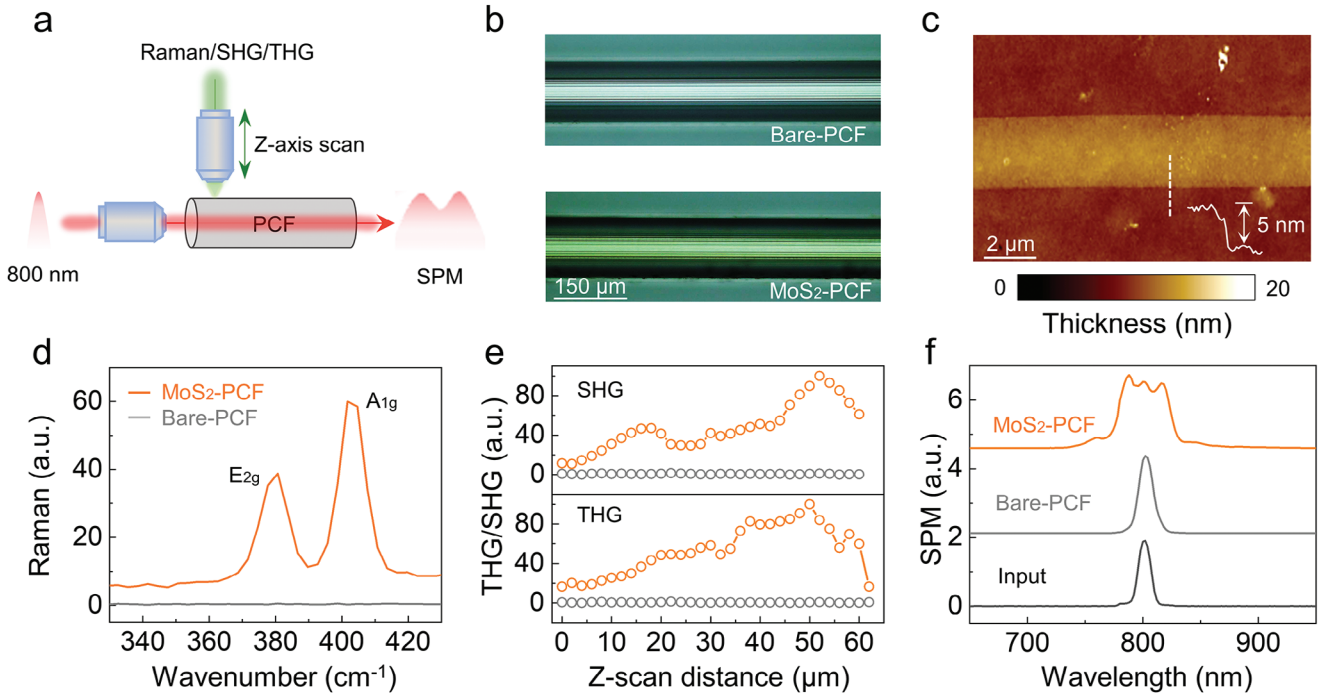

Figure 2. Characterizations of MoS_2-PCF. a) Schematic diagram of the experimental setup used to characterize the MoS_2-PCF. Pulsed light at 800 nm is incident horizontally into the fibre and the nonlinearity is obtained via measuring the spectral broadening caused by the SPM. In addition, continuous light at 532 nm, and pulsed light at 1064 nm and 1550 nm are used to measure the Raman, SHG and THG signals, respectively under excitation along the radial direction with z-axis scanning. b) Optical images of bare-PCF (top) and MoS_2-PCF (bottom). c) The AFM mapping of the collapsed MoS_2 tube after etching silica. The grown MoS_2 film is a quasi-bilayer with collapsed tube thickness of ≈5 nm (considering the probable presence of air-gap or wrinkles between tubes during the etching process). d) Raman spectra of PCF before and after growing MoS_2. The ≈21.0 cm^{-1} frequency difference between two peaks in MoS_2-PCF exhibits a successful growth of thin-layer MoS_2. e) Z-axis scanned SHG and THG intensity. Dramatically enhanced optical nonlinearity is obtained after growing MoS_2. f) SPM induced spectral broadening of bare- and MoS_2-PCF. The spectrum of MoS_2-PCF has more peaks and is wider than that of bare-PCF at 3 kW excitation pump power, indicating a higher nonlinear coefficient.

than 1% at 800 nm (Figure 1f and Experimental Section). This negligible propagation loss is expected due to the weak light scattering from the ultra-flatness of the 2D surface and small absorption of MoS_2 at ≈800 nm. With the wavelength decreases, it sustains ≈10% higher loss than that of the bare-PCF below 700 nm due to the increase of imaginary part of refractive index in MoS_2 (Figure S2a, Supporting Information). Thus, the improvement in nonlinearity with barely sacrificing dispersion and propagation loss is expected to substantially enhance the performance of SCG in PCF after thin-layer MoS_2 embedding.

Experimentally, the MoS_2-PCF is fabricated by a specially designed two-step method. This improved growth method can realize a good control of the thickness of embedded MoS_2 in the microstructured fibers (Experimental Section and Figure S6, Supporting Information). Optical images of the side views of PCF before and after MoS_2 growth are shown in **Figure** 2b. By using hydrofluoric acid to etch the silica-based fibre, the collapsed tube-packed MoS_2 film can be procured and analyzed by atomic force microscopy (AFM, Figure 2c). In order to gain a deeper understanding of both the sample quality and optical nonlinearity of the MoS_2-PCF, a custom-built optical system is established (Figure 2a), which allows for the simultaneous measurement of the Raman, SHG/THG and SPM spectra. From the Raman spectra, two fingerprint peaks of the MoS_2 (E_{2g} mode at 380.7 cm^{-1}, and A_{1g} mode at 401.7 cm^{-1}) can be clearly observed. The frequency difference of ≈21.0 cm^{-1} between these two peaks implies the successful growth of thin-layer MoS_2 (Figure 2d). By z-scanning measurement along the fibre radial direction, an obvious SHG/THG signal appears in the PCF after embedding MoS_2, which further reveals the efficient embedding of MoS_2 and indicates the integrated MoS_2 significantly amplifies the optical nonlinear effects of PCF (Figure 2e). This enhancement further promotes the nonlinear spectral broadening by the SPM effect, as shown in Figure 2f. According to the simulation results, the γ of MoS_2-PCF is close to 0.28 W^{-1} m^{-1}, which is 4.8 times larger than that of bare-PCF (Figure S7, Supporting Information).

Intuitively, the boosted SHG/THG and SPM with MoS_2 film embedded will enhance SCG in PCF. To quantify the impact of MoS_2 on the performance of SCG, we test the SCG evolution of bare-PCF and PCF embedded with a thin MoS_2 film (≈5 nm thickness of collapsed MoS_2 tube, as depicted in Figure 2c), under femtosecond laser pump at 800 nm (76 MHz repetition rate, ≈130 fs pulse width, the experimental setup is depicted in Experimental Section and Figure S8, Supporting Information). As expected, the SCG of the MoS_2-PCF exhibits a significantly enhancement compared with that of the bare-PCF (**Figure** 3a,b). For a straightforward comparison of the SCG broadening, we show their instantaneous spectra at three representative pump peak powers (Figure 3d). (*i*) At 4 kW, the bare-PCF maintains in the initial SPM stage, while the spectral evolution in the MoS_2-PCF

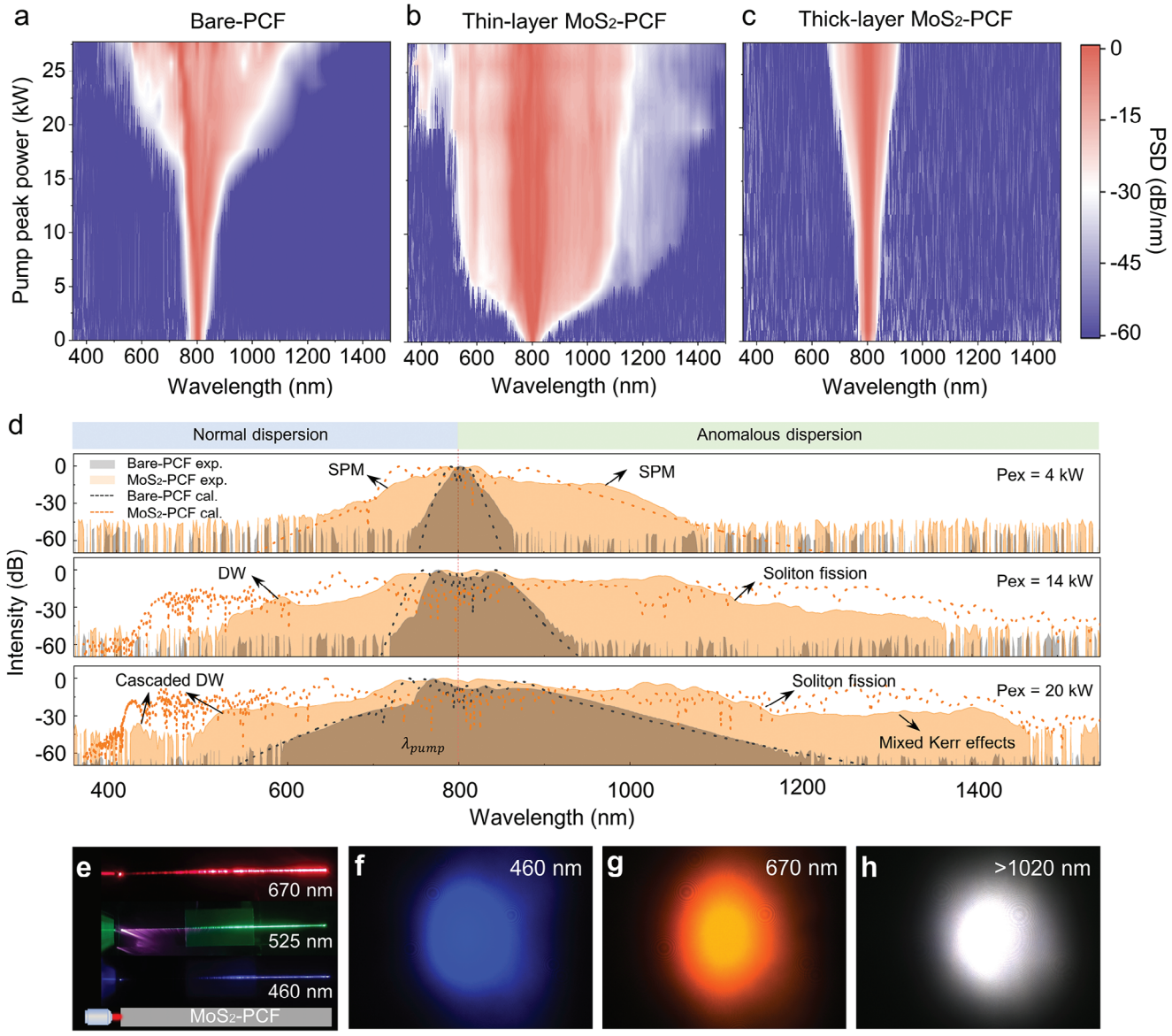

Figure 3. SCG evolution of MoS_2-PCF. a–c) Spectral evolution profiles of the bare-, thin-layer MoS_2- and thick-layer MoS_2-PCF under 800 nm pulsed laser pump. The pump peak power required to initiate soliton fission in the bare- and thin-layer MoS_2-PCF are ≈20 and ≈4 kW, respectively. The embedded thin MoS_2 film enhances the SCG broadening significantly, while the thick MoS_2 film suppresses the SCG broadening. d) Experimental and simulated instantaneous spectra of bare- and thin-layer MoS_2-PCF at three representative powers (4, 14, and 20 kW). Different spectral features are labeled (DW for dispersive wave). e) Side views along the fibre direction of the thin-layer MoS_2-PCF. Under the power of 20 kW, side views are recorded with bandpass filters of 670, 525 and 460 nm. The onset of soliton fission is observed at ≈1.2 cm, with spectral broadening to the visible range and cascaded DW generation of blue light at ≈1.5 cm. The length of MoS_2-PCF is 3 cm. Bottom panel shows the schematic setup. f–g) The output patterns from the MoS_2-PCF. The Gaussian-like spot indicates that the output beam has high quality at different wavelengths.

already starts the soliton fission process. (*ii*) At 14 kW, multiple spectral peaks due to SPM effect start to appear in the bare-PCF, while the spectrum in the MoS_2-PCF has already achieved one-octave spanning. (*iii*) At 20 kW, both fibers undergo the soliton fission process. The MoS_2-PCF exhibits a 1.8-octave SCG, which is significantly broader than the nearly one octave spectrum obtained from the bare-PCF. We note that the spectrum of the pump pulse used here spans the fiber's ZDW, thus the soliton number is invalid due to the combined dispersion regime. The SPM effect governs the initial pump pulse evolution until its spectrum significantly reaches the anomalous dispersion regime, where soliton dynamics, such as high-order soliton compression and soliton fission, start to dominate the evolution. Dispersive wave and mixed Kerr effects, such as four-wave mixing and cross phase modulation, further broaden the spectrum on both the longer and shorter wavelength side after soliton fission. The spectrum profile presents remarkable asymmetric characteristic, that is, the spectral components in the longer wavelength side are broadened more significantly. Details about the pulse duration characterization are given in Figure S9, Supporting Information.

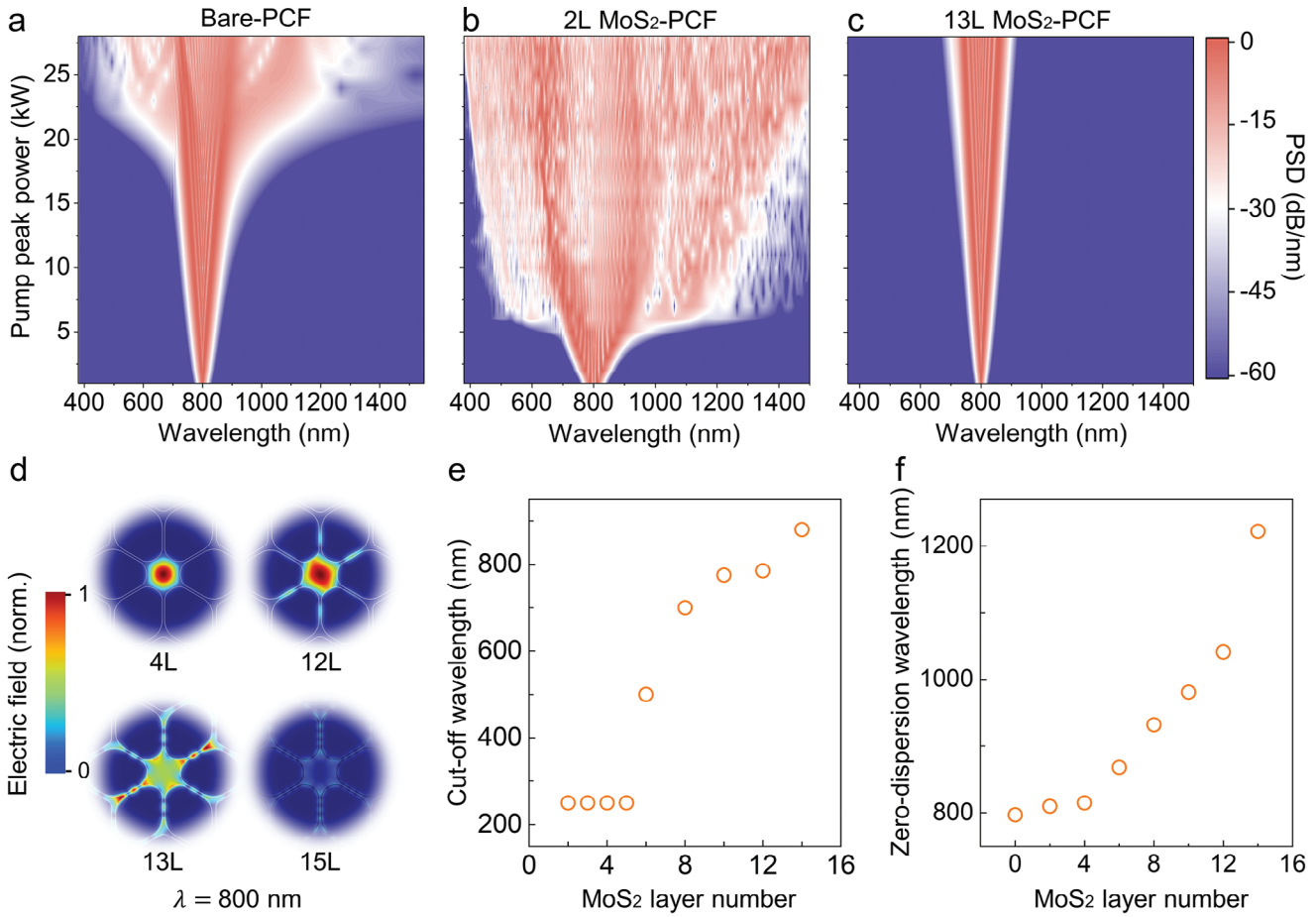

Figure 4. Simulations of the layer-dependent SCG performance in MoS_2-PCF. a–c) Simulations of the SCG spectrum evolution in bare-PCF a), bilayer MoS_2-PCF b) and 13-layer MoS_2-PCF c), under 800 nm pump. d) Fundamental mode profiles at 800 nm in MoS_2-PCF with different MoS_2 layer number. At a critical layer number of 12, light gradually diffuses from the core region to the cladding area until nearly disappears at 15 layers. e) The cut-off wavelength (defined as the ability to keep fundamental mode intensity intact) versus MoS_2 layer number. For the SCG broadening to cover the visible part of ≥400 nm, the MoS_2 layer number should be ≤5. f) The dependence of ZDW on MoS_2 layer number. ZDW red-shifts away from the pump wavelength of 800 nm with the layer number increasing.

We find a 70% reduction in the threshold power required to attain a one-octave-spanning spectrum in MoS_2-PCF, while maintaining the stability of output beam profile (Figure S10, Supporting Information).

The small scattered portion of guided light out of the fibre by embedded MoS_2 film enables us to directly observe the whole process of the SCG evolution (Figure 3e). At the beginning, the pump field undergoes initial SPM process and gradually broadens to visible red light. Then the spectrum suddenly becomes octave spanning through soliton fission and dispersive wave generation processes, leading to the wavelength conversion of the pump light to green and blue regimes. Almost all output light components at different wavelengths show optical field patterns with Gaussian-like field distribution pattern (Figure 3f–h). This facilitates a lower coupling loss and higher spot quality when the generated supercontinuum is coupled to other optical systems (e.g., single-mode fibers, objective lenses, etc.).

However, the SCG enhancement is not adaptable to the MoS_2 layer with arbitrary thickness. As we test a thick-layer MoS_2-PCF with measured collapsed MoS_2 tube film thickness of ≈20 nm (Figure S11, Supporting Information), the SCG broadening is dramatically suppressed compared to that of the bare-PCF (Figure 3c). The distinct performance of the thin-layer and thick-layer MoS_2 hints a layer-dependent SCG performance. In the following, we conduct numerical calculations to comprehend this layer-dependent SCG behavior in MoS_2-PCFs. The evolution of SCG is simulated by numerically solving a generalized nonlinear Schrödinger equation (GNLSE) (Note S2, Supporting Information), which is widely used for modelling SCG and enables accurate prediction of the spectral dynamics of ultrashort pulse propagation in nonlinear fibers.[49] We simulate SCG in the bare-PCF at first (**Figure 4a**), and find its result matches well with our experimental result in Figure 3a. After embedding MoS_2 into the PCF, the SCG spectra of bilayer MoS_2-PCF (Figure 4b) shows pronounced enhancements, agreeing well with the experimental result of thin-layer MoS_2-PCF (Figure 3b). As the thickness of MoS_2 increases to 13 layers, the spectrum range of SCG is suppressed in contrast (Figure 4c). These simulations reproduce well the experiments of layer-dependent SCG enhancement in the MoS_2-PCF, and

suggest the existence of a critical layer for achieving the optimal SCG enhancement.

To further elucidate the origin of the layer-dependent enhancement and delimit the critical layer number of embedded MoS_2, we systematically analyze the transmission mode, ZDW and nonlinear coefficient with different layer number of MoS_2 (Figure 4d–f and Figure S12, Supporting Information). For the transmission mode of the hybrid PCF, the effective refractive index of fibre cladding rises correspondingly with the embedded MoS_2 thickness until surpassing that of fibre core and breaking the total internal reflection condition. As a result, the light bundled at the core area gradually diffuses into the cladding region and leads to a significant leakage loss. For example, the fundamental mode of transmission wavelength at 800 nm is kept stable before 12 layers but exhibits an obvious diffusion since 13 layers (Figure 4d). Thus, there is a cut-off wavelength for MoS_2-PCFs under a specific layer number, at which the fundamental mode of a shorter wavelength cannot be transmitted in the fibre. As the MoS_2 layer number decreases, this cut-off wavelength undergoes a blueshift and drops out of the visible spectrum range at a critical layer around five (Figure 4e). It should be noted that the calculated cut-off wavelength of ≈250 nm for the case of ≤5 layers is due to the absorption of fused-silica itself. Moreover, the layer-dependent mode diffusion breaks the monotonous increase of the nonlinear coefficient with layer number and a maximum value is achieved at 12 layers (Figure S12, Supporting Information). As for the ZDW of the MoS_2-PCF, it red-shifts sharply away from the pump wavelength with the increase of MoS_2 layer number (Figure 4f). Thus, the original 800 nm pump wavelength falls into deep normal dispersion region, preventing the formation of optical solitons in the fibre and therefore limiting the spectral broadening in the SCG process.[8] Taking a comprehensive consideration, the γ of the PCF increases with the thickness of the embedded MoS_2 layer, but excessive thickness will lead to mode leakage and ZDW shift. Hence, MoS_2 layer number of around five is the optimal one for the enhancement of SCG with the visible to near-infrared spectral coverage in this hybrid PCF.

3. Conclusion

In summary, we have demonstrated an effective methodology to enhance the SCG performance by embedding solid-state MoS_2 atomic layers into the air-holes of silica-based PCF. The corporation of a 2D material with a critical thickness endows the optical fibre with the optimal SCG output. Given the large library of 2D materials with diverse physical properties, our work indicates a way for extending SCG with wider spectrum, lower threshold power and better tunability. This non-destructive, portable and easy-to-integrate solution should promote the development of fibre-based table-top light sources.

4. Experimental Section

MoS_2-PCF Sample Growth: The MoS_2-PCF was prepared by the two-step CVD method. First, Na_2MoO_4 aqueous solution with optimized concentration (50 and 150 mg mL^{-1} for thin-layer and thick-layer MoS_2-PCFs fabrication, respectively) was filled into the needle tube and injected directly into the air-holes of PCF. Then the feedstock filled fibers were baked at 110 °C in the CVD furnace for ≈30 min to dewet and these Na_2MoO_4 deposited fibers were placed on the quartz plate and reloaded into the CVD furnace. Second, the Na_2MoO_4 precursor in fibre was gradually heated to 800 °C for ≈40 min and it started to react with sulphur vapour (here the S powder was heated at 150–180 °C by a heating belt separately) carried by argon gas (100 sccm) for homogeneous MoS_2 growth. This work maintained the ambient pressure at the heating stage to avoid the molten Na_2MoO_4 diffusing out of fibre and ensure sufficient Mo supply without early volatilization, and only pump the system into low-pressure at growth and cooling stages. It was worth noting that the supplied S source at the upstream was also utilized to match up with the timing of varied pressure in the procedure. The detailed growth setup and heating temperature profiles are provided in Figure S6a,b, Supporting Information. With this procedure, the grown thin-layer MoS_2-PCFs exhibited full MoS_2 coverage and consistency within a typical length of 6–7 cm (Figure S13, Supporting Information). In addition, for thick-layer MoS_2 grown in the air-hole of PCF, its thickness was controlled by adjusting the amount of pre-deposited Mo source. This was because the multilayer nucleation growth was mainly determined by the Mo precursors due to their poor volatility during the synthesis. As a result, the average thickness of MoS_2 was proportional to the pre-injected Na_2MoO_4 solution concentration (Figure S6c, Supporting Information).

MoS2-PCF Characterization: Optical images of bare-PCF and MoS_2-PCFs were obtained by an Olympus BX51M microscope. A home-made optical system was designed to measure Raman spectra and z-scanning SHG and THG, excited through a continuous laser at 514 nm and a picosecond pulsed laser at 1064 and 1550 nm, respectively. The SPM spectral broadening was obtained by the horizontal incidence of an 800 nm pulsed laser (130 fs pulse width, 76 MHz repetition) launching into the core region of PCFs. Collapsed MoS_2 tube samples for the AFM (Bruker Dimensional Icon) test were prepared by immersing MoS_2-PCF in hydrofluoric acid to dissolve the silica, and then transferring the MoS_2 tube samples onto the substrate. A laser line filter (NKT) was used to select the monochromatic light from a supercontinuum laser (NKT, WL-SC-400-4) to perform the transmission measurement. Starting from 450 nm, wavelengths at 10 nm interval were selected out. Light is coupled into the fibre through an objective (Olympus, ×40, NA = 0.65) and its power before and after the incidence into the fibre was measured by an optical power meter (Thorlabs, PM100D and S120VC), from which the transmittance was obtained. The transmission results shown in Figure 1f have been calibrated by eliminating the coupling loss from the objective lens (Figure S14, Supporting Information).

Supercontinuum Generation Experiments: A titanium-sapphire oscillator (Coherent, Mira-HP, 800 nm, specifications mentioned before) was used as excitation laser and light was coupled into optical fibre samples via an objective (Olympus, ×40, NA = 0.65). The cross-section of the fibre was observed by using white light imaging system to verify the incident pulse laser was aligned with the fibre core. The output supercontinuum light source was collected by YOKOGAWA AQ6374 spectrometer via a transmission system. The output power was collected by a thermal power sensor (Thorlabs, S401C). Pictures of the side views of the MoS_2-PCF glowing at various wavelengths were filtered by a series of band pass filters and taken via a charge-coupled device camera. The experimental setup was schemed in Figure S8, Supporting Information.

Numerical Simulations: The simulations were performed using the RF module of COMSOL Multiphysics software and MATLAB software. The intensity distribution and effective refractive index of the fundamental mode in bare- and MoS_2-PCFs were simulated using the finite element method in COMSOL. In the model, all the air-holes in the PCF were covered by layered MoS_2. To eliminate the reflection effect of the leaky light on the mode shape, this work considered perfectly matched layer and scattering boundary condition in the simulation process. The relative intensity of MoS_2 was defined as the ratio of the electric field intensity at the innermost MoS_2 position to that at the fibre core center along the x-axis (Figure 1b,c). The electric field intensity was calculated by $E = \sqrt{E_x^2 + E_y^2}$, where E_x and E_y are the intensity of two orthogonal fundamental modes, respectively. Based on these simulating results, the dispersion and nonlinear coefficient of the bare- and MoS_2-PCFs were calculated, respectively. The SCG in bare- and MoS_2-PCFs was simulated by using the GNLSE. The

fourth-order Runge-Kutta algorithm was used to numerically calculate the GNLSE in the frequency domain. More details can be found in Note S2, Supporting Information.

Supporting Information

Supporting Information is available from the Wiley Online Library or from the author.

Acknowledgements

This work was supported by the National Natural Science Foundation of China (52025023, 52021006, 52203331, 51991342, 12374167, T2188101, 92163206, 11888101, 62075188, 62375131), Beijing Municipal Science and Technology Commission (Z221110004500000), National Key R&D Program of China (2021YFB3200303, 2021YFA1400201, 2021YFA1400502 and 2022YFA1403504), Guangdong Major Project of Basic and Applied Basic Research (2021B0301030002), the Strategic Priority Research Program of Chinese Academy of Sciences (XDB33000000).

Conflict of Interest

The authors declare no conflict of interest.

Author Contributions

J.X., X.C., G.X., and X.L. contributed equally to this work. Kaihui Liu, Z.L., H.H., and Z.K. conceived the experiments and supervised the project. G.X., D.Z., and Y.Z. performed the growth experiments. J.X., G.X., and K.L. conducted the Raman and SHG characterizations. J.X. and W.Y. performed the SCG experiments. X.C., Z.K., and X.L. contributed to the theoretical modelling. H.H., C.L., X.J., M.P., and Z.S. suggested the optical experiments. K.L., H.H., J.X., and X.C. wrote the manuscript. All authors contributed to the scientific discussion and modifying the manuscript.

Data Availability Statement

The data that support the findings of this study are available from the corresponding author upon reasonable request.

Keywords

2D materials, nonlinear optics, optical fiber, supercontinuum generation

Received: March 12, 2024
Revised: June 15, 2024
Published online:

[1] C. Gmachl, D. L. Sivco, R. Colombelli, F. Capasso, A. Y. Cho, *Nature* **2002**, *415*, 883.
[2] F. Silva, D. R. Austin, A. Thai, M. Baudisch, M. Hemmer, D. Faccio, A. Couairon, J. Biegert, *Nat. Commun.* **2012**, *3*, 807.
[3] H. Guo, C. Herkommer, A. Billat, D. Grassani, C. Zhang, M. H. P. Pfeiffer, W. Weng, C.-S. Brès, T. J. Kippenberg, *Nat. Photonics* **2018**, *12*, 330.
[4] G. Vicidomini, P. Bianchini, A. Diaspro, *Nat. Methods* **2018**, *15*, 173.
[5] H. Ren, L. Shen, A. F. J. Runge, T. W. Hawkins, J. Ballato, U. Gibson, A. C. Peacock, *Light Sci Appl* **2019**, *8*, 105.
[6] X. Ji, D. Mojahed, Y. Okawachi, A. L. Gaeta, C. P. Hendon, M. Lipson, *Sci. Adv.* **2021**, *7*, eabg8869.
[7] R. R. Alfano, *The Supercontinuum Laser Source: The Ultimate White Light*, Springer, Cham **2022**.
[8] J. M. Dudley, G. Genty, S. Coen, *Rev. Mod. Phys.* **2006**, *78*, 1135.
[9] J. Herrmann, U. Griebner, N. Zhavoronkov, A. Husakou, D. Nickel, J. C. Knight, W. J. Wadsworth, P. S.t. J. Russell, G. Korn, *Phys. Rev. Lett.* **2002**, *88*, 173901.
[10] W. H. Reeves, D. V. Skryabin, F. Biancalana, J. C. Knight, P. S.t. J. Russell, F. G. Omenetto, A. Efimov, A. J. Taylor, *Nature* **2003**, *424*, 511.
[11] A. V. Husakou, J. Herrmann, *Phys. Rev. Lett.* **2001**, *87*, 203901.
[12] A. V. Gorbach, D. V. Skryabin, *Nat. Photonics* **2007**, *1*, 653.
[13] J. M. Dudley, J. R. Taylor, *Supercontinuum Generation in Optical Fibers*, Cambridge University Press, Cambridge **2010**.
[14] V. V. R. Kumar, A. George, W. Reeves, J. Knight, P. Russell, F. Omenetto, A. Taylor, *Opt. Express* **2002**, *10*, 1520.
[15] C. R. Petersen, U. Møller, I. Kubat, B. Zhou, S. Dupont, J. Ramsay, T. Benson, S. Sujecki, N. Abdel-Moneim, Z. Tang, D. Furniss, A. Seddon, O. Bang, *Nat. Photonics* **2014**, *8*, 830.
[16] X. Jiang, N. Y. Joly, M. A. Finger, F. Babic, G. K. L. Wong, J. C. Travers, P. S.t. J. Russell, *Nat. Photonics* **2015**, *9*, 133.
[17] Z. Eslami, L. Salmela, A. Filipkowski, D. Pysz, M. Klimczak, R. Buczynski, J. M. Dudley, G. Genty, *Nat. Commun.* **2022**, *13*, 2126.
[18] Y. Ohishi, *Opt. Mater. Express* **2022**, *12*, 3990.
[19] F. Couny, F. Benabid, P. J. Roberts, P. S. Light, M. G. Raymer, *Science* **2007**, *318*, 1118.
[20] P. S. Russell, P. Holzer, W. Chang, A. Abdolvand, J. C. Travers, *Nat. Photonics* **2014**, *8*, 278.
[21] M. Chemnitz, M. Gebhardt, C. Gaida, F. Stutzki, J. Kobelke, J. Limpert, A. Tünnermann, M. A. Schmidt, *Nat. Commun.* **2017**, *8*, 42.
[22] C. Markos, J. C. Travers, A. Abdolvand, B. J. Eggleton, O. Bang, *Rev. Mod. Phys.* **2017**, *89*, 045003.
[23] R. Sollapur, D. Kartashov, M. Zürch, A. Hoffmann, T. Grigorova, G. Sauer, A. Hartung, A. Schwuchow, J. Bierlich, J. Kobelke, M. Chemnitz, M. A. Schmidt, C. Spielmann, *Light Sci. Appl.* **2017**, *6*, e17124.
[24] U. Elu, L. Maidment, L. Vamos, F. Tani, D. Novoa, M. H. Frosz, V. Badikov, D. Badikov, V. Petrov, P. St. J. Russell, J. Biegert, *Nat. Photonics* **2021**, *15*, 277.
[25] A. K. Geim, K. S. Novoselov, *Nat. Mater.* **2007**, *6*, 183.
[26] F. Bonaccorso, Z. Sun, T. Hasan, A. C. Ferrari, *Nat. Photonics* **2010**, *4*, 611.
[27] K. F. Mak, C. Lee, J. Hone, J. Shan, T. F. Heinz, *Phys. Rev. Lett.* **2010**, *105*, 136805.
[28] G. Cassabois, P. Valvin, B. Gil, *Nat. Photonics* **2016**, *10*, 262.
[29] J. D. Caldwell, I. Aharonovich, G. Cassabois, J. H. Edgar, B. Gil, D. N. Basov, *Nat. Rev. Mater.* **2019**, *4*, 552.
[30] F. N. Xia, H. Wang, D. Xiao, M. Dubey, A. Ramasubramaniam, *Nat. Photonics* **2014**, *8*, 899.
[31] Y. Wu, Q. Wu, F. Sun, C. Cheng, S. Meng, J. Zhao, *Proc. Natl. Acad. Sci. U. S. A.* **2015**, *112*, 11800.
[32] S. Karmakar, S. Biswas, P. Kumbhakar, *Opt. Spektrosk. (Akad. Nauk SSSR, Otd. Fiz.-Mat. Nauk)* **2017**, *73*, 585.
[33] K. S. Novoselov, A. Mishchenko, A. Carvalho, A. Castro Neto, *Science* **2016**, *353*, aac9439.
[34] I. Datta, S. H. Chae, G. R. Bhatt, M. A. Tadayon, B. Li, Y. Yu, C. Park, J. Park, L. Cao, D. N. Basov, J. Hone, M. Lipson, *Nat. Photonics* **2020**, *14*, 256.
[35] B. Yao, S.-W. Huang, Y. Liu, A. K. Vinod, C. Choi, M. Hoff, Y. Li, M. Yu, Z. Feng, D.-L. Kwong, Y. Huang, Y. Rao, X. Duan, C. W. Wong, *Nature* **2018**, *558*, 410.

[36] Y. Zhang, J. Wu, L. Jia, Y. Qu, Y. Yang, B. Jia, D. J. Moss, *Laser Photonics Rev.* **2023**, *17*, 2200512.
[37] J. h. Chen, Y.-f. Xiong, F. Xu, Y. q. Lu, *Light Sci Appl* **2021**, *10*, 78.
[38] A. Autere, H. Jussila, Y. Dai, Y. Wang, H. Lipsanen, Z. Sun, *Adv. Mater.* **2018**, *30*, 1705963.
[39] Q. Bao, H. Zhang, Y.u Wang, Z. Ni, Y. Yan, Z.e X. Shen, K. P. Loh, D. Y. Tang, *Adv. Funct. Mater.* **2009**, *19*, 3077.
[40] Y. Zuo, W. Yu, C. Liu, X.u Cheng, R. Qiao, J. Liang, X.u Zhou, J. Wang, M. Wu, Y. Zhao, P. Gao, S. Wu, Z. Sun, K. Liu, X. Bai, Z. Liu, *Nat. Nanotechnol.* **2020**, *15*, 987.
[41] G. Q. Ngo, E. Najafidehaghani, Z. Gan, S. Khazaee, M. P. Siems, A. George, E. P. Schartner, S. Nolte, H. Ebendorff-Heidepriem, T. Pertsch, A. Tuniz, M. A. Schmidt, U. Peschel, A. Turchanin, F. Eilenberger, *Nat. Photonics* **2022**, *16*, 769.
[42] N. Vermeulen, D. Castelló-Lurbe, M. Khoder, I. Pasternak, A. Krajewska, T. Ciuk, W. Strupinski, J. Cheng, H. Thienpont, J. Van Erps, *Nat. Commun.* **2018**, *9*, 2675.
[43] K.e Chen, X.u Zhou, X.u Cheng, R. Qiao, Y.i Cheng, C. Liu, Y. Xie, W. Yu, F. Yao, Z. Sun, F. Wang, K. Liu, Z. Liu, *Nat. Photonics* **2019**, *13*, 754.
[44] D. Erkensten, S. Brem, E. Malic, *Phys. Rev. B* **2021**, *103*, 045426.
[45] C. Louca, A. Genco, S. Chiavazzo, T. P. Lyons, S. Randerson, C. Trovatello, P. Claronino, R. Jayaprakash, X. Hu, J. Howarth, K. Watanabe, T. Taniguchi, S. Dal Conte, R. Gorbachev, D. G. Lidzey, G. Cerullo, O. Kyriienko, A. I. Tartakovskii, *Nat. Commun.* **2023**, *14*, 3818.
[46] G. A. Ermolaev, Y. V. Stebunov, A. A. Vyshnevyy, D. E. Tatarkin, D. I. Yakubovsky, S. M. Novikov, D. G. Baranov, T. Shegai, A. Y. Nikitin, A. V. Arsenin, V. S. Volkov, *NPJ 2D Mater Appl* **2020**, *4*, 21.
[47] F. Liu, X. Zhao, X.-Q. Yan, X. Xin, Z.-B.o Liu, J.-G. Tian, *Appl. Phys. Lett.* **2018**, *113*, 051901.
[48] Q. Ouyang, K. Zhang, W. Chen, F. Zhou, W. Ji, *Opt. Lett.* **2016**, *41*, 1368.
[49] G. P. Agrawal, *Nonlinear Fiber Optics*, Academic Press, Cambridge **2019**.